Yves Olsommer* and Frank R. Ihmig

Passive control strategy of inductive power transfer to microimplants based on ferroelectric dielectrics

https://doi.org/10.1515/ cdbme-2024-2116

Abstract: In this study, a passive control strategy of inductive power transfer (IPT) using ferroelectric multilayer ceramic chip capacitors (MLCCs) is presented. The required system parameters, i.e., ferroelectric hysteresis, frequency of the IPT, and voltage range across the MLCCs are reported. The receiver circuit consists only of a parallel resonant circuit, a half-wave rectifier and a load; the passive control of the IPT is achieved exclusively by the nonlinear properties of the ferroelectric MLCCs. The stabilization of the secondary output voltage U_{Load} at constant load is experimentally evaluated for an inductive coupling factor k between 10 % and 30 % for three nonlinear MLCCs #1, #2 and #3. With our proposed passive control strategy U_{Load} is maintained at -1.2 % and +0.6 % around a median value of 17.3 V (17.1 - 17.4 V) for $k \in [20\ \%, 30\ \%]$ using MLCC #1, ±0.9 % around a median value of 11.2 V (11.1 - 11.3 V) for $k \in [10\ \%, 18\ \%]$ using MLCC #2, and -1.6% and +2.6 % around a median value of 5.03 V (4.95 - 5.16 V) for $k \in [16\ \%, 30\ \%]$ using MLCC #3. The proposed control principle is particularly advantageous for highly miniaturized microimplants, as it allows IPT control without additional semiconductors, sensors and vulnerable communication channels.

Keywords: inductive power transfer, passive control, nonlinear capacitance, ferroelectric MLCCs, smart material, microimplants.

1 Introduction

Most neurostimulators currently on the market for the treatment of drug-resistant and therapy-refractory disorders (e.g., epilepsy, Parkinson's disease, obsessive-compulsive disorder, overactive bladder, obstructive sleep apnea) have a limited lifespan due to product-related adverse events [1] and limited battery life [2]. The most common product-related adverse events include migration and fracture of the leads between the neurostimulator and stimulation electrodes, as well as stimulator malfunction [1]. These adverse events result in additional surgical procedures, exposing patients who already belong to a frail population to additional risk and additional cost [2].

As a result, leadless and battery-free neurostimulators have been developed in recent years. One example is the Genio® hypoglossal nerve stimulator (Nyxhoa SA, Mont-Saint-Guibert, Belgium) [3], approved for the European market in 2019 to treat obstructive sleep apnea [4]. This stimulator consists only of a coil, capacitors, diodes, resistors and stimulation electrodes [5].

These stimulators are powered by IPT. A time-varying magnetic field is generated via the coil of an extracorporeal transmitter, inducing a voltage across the coil of the stimulator. The sole function of the stimulator is to convert the induced voltage into a stimulation pulse. The width and repetition rate of the stimulation pulses are set by the extracorporeal transmitter, while the amplitude depends on 1) the inductively transmitted power, 2) the electrode impedance, and 3) the inductive coupling factor. The amplitude of the stimulation pulse must be kept within a safe range to ensure successful therapy [6] and patient safety [7].

Closed-loop control methods are generally used to overcome this challenge. This requires data exchange between the secondary stimulator and the primary extracorporeal transmitter [8]. In this way, a change in the electrode impedance (the load) [9] and the inductive coupling factor can be compensated for by adjusting the power fed to the primary coil [8]. However, this approach is not suitable for the simply designed microimplants described above, as additional semiconductors, sensors and vulnerable communication channels are required.

Another approach is to use compensation circuits, such as a series-series circuit, to make the IPT either load-independent [10] or independent of the inductive coupling factor [11]. In

***Corresponding author: Yves Olsommer:** Saarland University, Campus, Saarbrücken 66123, Germany, e-mail: yves.olsommer@ibmt.fraunhofer.de
Frank R. Ihmig: Fraunhofer Institute for Biomedical Engineering, Sulzbach/Saar 66280, Germany

practice, however, additional control methods are required [10, 11].

In this paper, we aim to use ferroelectric dielectrics of MLCCs as smart materials to realize passive control of IPT. Passive control of the secondary output voltage is experimentally demonstrated for three MLCCs over a given coupling factor range and for a constant load.

First, the selected ferroelectric MLCCs and the measurement setup for IPT characterization are presented in sections 2.1 and 2.2, respectively. The measured hysteresis of each nonlinear MLCC is then presented in section 3.1, followed by the IPT characterization in section 3.2. Finally, the results are summarized in section 4.

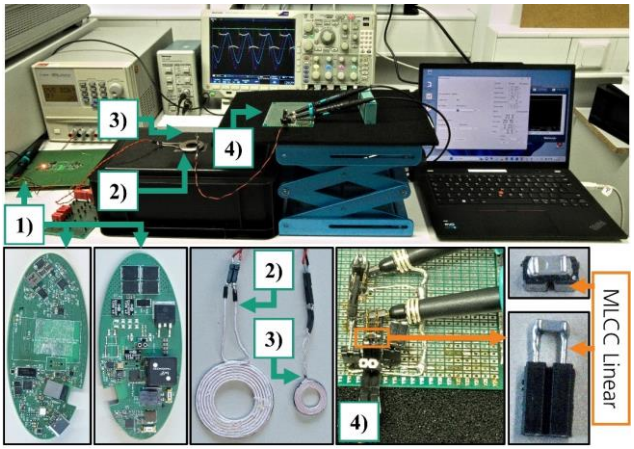

Figure 1: Measurement setup to characterize the IPT consisting of an extracorporeal transmitter 1) to drive the primary coil 2). A voltage is induced at the secondary coil 3) and rectified by the receiver circuit 4). The inductive coupling factor is varied by changing the distance between both coils using the laboratory lift.

2 Material and Methods

2.1 Selected MLCCs

The IPT is characterized for three ferroelectric (class 2) MLCCs #1, #2 and #3 and a paraelectric (class 1) MLCC Linear for reference. A detailed description of these MLCCs is given in Table 1.

Table 1: Manufacturer's part number, nominal capacitance, rated voltage, case size and temperature coefficient of each MLCC.

MLCC	Part number	Description
Linear	GRM31M5C1H473JA01L	47 nF, 50 V, 1206, C0G
#1	0402F473Z250CT	47 nF, 25 V, 0402, Y5V
#2	MC0805F473Z500CT	47 nF, 50 V, 0805, Y5V
#3	GRM022R60J473ME15L	47 nF, 6.3 V, 01005, X5R

2.2 Measurement setup

The measurement setup shown in Figure 1 is used to characterize the IPT. The primary series resonant circuit with the coil 2) is driven by the extracorporeal transmitter 1) through a half-bridge. The extracorporeal transmitter is supplied with a voltage of 4.2 V using the U8031A power supply unit (Agilent Technologies Inc., Santa Clara, CA, USA). The frequency of the IPT and the voltage at the half-bridge can be adjusted via Bluetooth®. The secondary receiver unit 4) consists of a parallel resonant circuit with the coil 3), a half-wave rectifier and a load of 1200 Ω. The parallel resonant circuit contains the nonlinear ferroelectric MLCCs used for passive control of the IPT.

The laboratory lift is used to change the distance between the primary and secondary coils and thus the inductive coupling factor. The coupling factor is determined using an Agilent 4294A precision impedance analyzer. The secondary voltage at the load U_{Load} is measured using an MDO4104-6 oscilloscope (Tektronix Inc., Beaverton, OR, USA) and a TT-MF312-2-6 11020-2-6 probe (TESTEC Elektronik GmbH, Frankfurt, Germany) and transferred to a computer using the Tektronix OpenChoice Desktop software.

The inductance and loss resistance of the primary and secondary coils are measured with the Agilent 4294A impedance analyzer and are listed in Table 2, along with the resonance frequency of both resonant circuits and the capacitance of the primary series resonant circuit.

Table 2: Inductance and loss resistance of the primary (L_1 and R_1) and secondary (L_2 and R_2) coils. Different resonant frequencies f_{res} result for each MLCC. The corresponding capacitance of the primary series resonant circuit is indicated by C_1. All measurements were performed at the corresponding f_{res}.

MLCC	L_1 [µH]	R_1 [Ω]	C_1 [nF]	L_2 [µH]	R_2 [Ω]	f_{res} [kHz]
Linear	6,24	0,26	28,06	3,90	0,24	370
#1	6,24	0,29	19,56	3,90	0,26	438
#2	6,24	0,26	27,93	3,90	0,24	368
#3	6,24	0,30	18,02	3,90	0,27	459

3 Results

3.1 Measured ferroelectric hysteresis

To characterize the nonlinearity of the MLCCs, the electric charge q in the dielectric is measured as a function of the voltage u applied across the dielectric using a Sawyer-Tower circuit [12]. The u-q characteristics of each MLCC are shown in Figure 2.

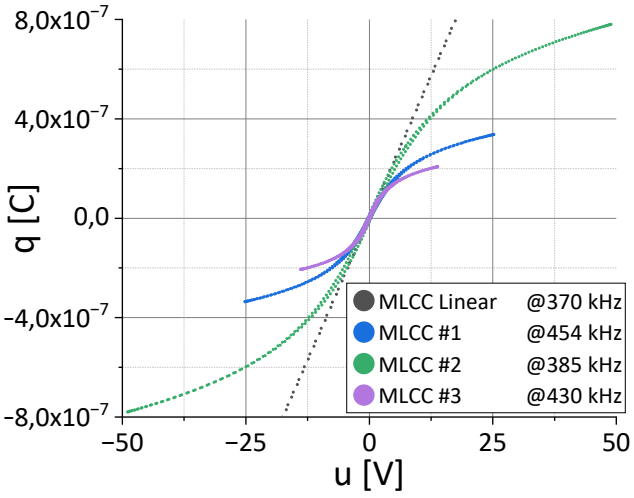

Figure 2: u-q characteristics of the linear paraelectric MLCC Linear and the nonlinear ferroelectric MLCCs #1, #2 and #3 measured with a Sawyer-Tower circuit.

A linear relationship between the electric charge q and the voltage u can be observed in Figure 2 for the paraelectric MLCC Linear. For the ferroelectric MLCCs #1, #2 and #3, the relationship between u and q is nonlinear, i.e., unlike the linear MLCC, the resulting capacitance is voltage-dependent.

The ferroelectric hysteresis of MLCC #1, #2 and #3 has a linear region at low voltages, a transition region, and a nonlinear region at higher voltages. For example, for MLCC #2, these regions are in a voltage range of around ±10 V, between ±10 V and ±25 V, and above ±25 V, respectively.

The measured u-q characteristics in Figure 2 are used to determine the material parameters of the respective dielectrics, which are the input parameters of our physics-based model. A detailed description of the material parameter extraction and the physics-based model can be found in [13].

3.2 Experimental characterization of IPT

The selection of the ferroelectric MLCCs and the system design, including 1) the capacitance of the primary series resonant circuit, 2) the frequency of the IPT, and 3) the voltage range across the ferroelectric MLCC of the secondary parallel resonant circuit, are determined using our physics-based model [13].

To characterize the IPT, the secondary voltage U_{Load} at a load of 1200 Ω is shown in Figure 3 as a function of the inductive coupling factor k.

The measurements with the paraelectric MLCC Linear are used as a reference and show how a change in the inductive coupling factor k impacts the secondary voltage U_{Load} in conventional IPT systems without any closed-loop control. Paraelectric MLCCs exhibit a linear relationship between the electric charge stored in the dielectric and the applied voltage (see Figure 2, black); resulting in a voltage-independent capacitance. As the inductive coupling factor k changes, the mutual inductance also changes, causing the primary and secondary resonant circuits to detune each other. As a result, a strong dependence between the secondary voltage U_{Load} and the inductive coupling factor k can be seen in Figure 3 with MLCC Linear at resonance (black) and 44 kHz above resonance (red). In resonance, a maximum secondary voltage U_{Load} of 21.5 V is achieved at an inductive coupling factor k of 4.2 %. However, if the IPT is performed 44 kHz above resonance, the mutual inductance at an inductive coupling factor k of 24.4% brings both resonant circuits into resonance with a maximum secondary voltage U_{Load} of 18.4 V.

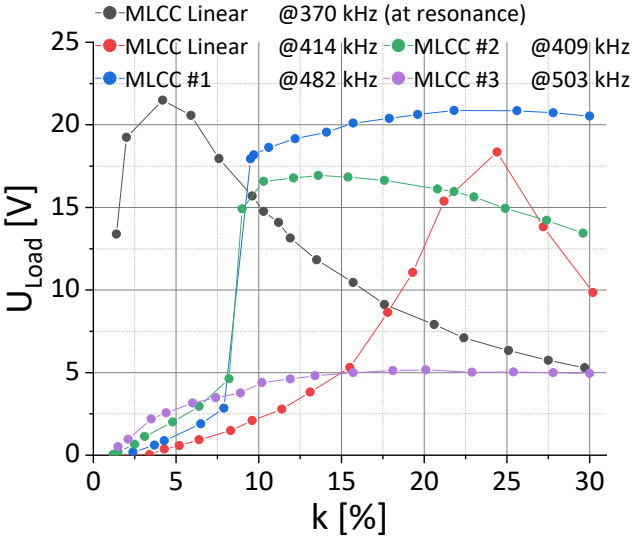

Figure 3: Secondary voltage U_{Load} at a load of 1200 Ω as a function of the inductive coupling factor k for the linear MLCC Linear at resonance (black) and 44 kHz above resonance (red), as well as for the nonlinear ferroelectric MLCCs #1 (blue), #2 (green) and #3 (purple). The IPT is performed using MLCCs #1, #2 and #3 respectively at 44, 41 and 44 kHz above the resonance frequency of the primary and secondary resonant circuits.

In contrast to paraelectric linear MLCCs, the relationship between the electric charge stored in the dielectric and the applied voltage is nonlinear in ferroelectric MLCCs (see Figure 2), resulting in a voltage-dependent capacitance. Thus, the capacitance of the secondary resonant circuit is a function of the induced voltage. In this case, the secondary resonant circuit is detuned not only by the mutual inductance, but also by the voltage-dependent capacitance. Ideally, the nonlinearity of the ferroelectric hysteresis should be designed so that the resulting voltage-dependent capacitance compensates for the changing mutual inductance over a defined range of the inductive coupling factor. In this work, we used the ferroelectric hysteresis of commercially available MLCCs.

To achieve the highest possible stabilization of the secondary voltage U_{Load} over a range of the inductive coupling factor k between 10 % and 30 %, our physics-based model [13] was used to identify MLCCs with suitable ferroelectric hysteresis for passive control of the IPT and to determine the required system parameters, namely 1) the frequency of the IPT, and 2) the voltage range across the MLCCs.

The IPT system, consisting of the primary series resonant circuit and the secondary parallel resonant circuit including the nonlinear MLCC for passive power control, is operated with nonlinear MLCCs #1, #2, and #3 respectively at 44, 41, and 44 kHz above its resonance frequency. For an inductive coupling factor $k < 10$ %, the system is operated out of resonance. Here, as the inductive coupling factor increases, both the mutual inductance and, for $k < 10$ %, the voltage induced on the secondary resonant circuit increase. Once the induced voltage at the nonlinear MLCCs reaches a specific value, the mutual inductance is compensated in such a way that the system swings into resonance, resulting in a sharp increase in the secondary voltage U_{Load}. This sharp increase in U_{Load} can be observed particularly with MLCCs #1 and #2 between a coupling factor of 7.9 % and 9.5 %. If the mutual inductance is over- or undercompensated by the voltage-dependent nonlinear capacitance at higher coupling factors, the stabilization effect of the secondary voltage U_{Load} will be reduced (see Figure 3, MLCC #1 and #2). In other words, a particularly high stabilization of U_{Load} is only possible over a limited range of the inductive coupling factor k using the ferroelectric hysteresis of commercially available MLCCs.

The power of the extracorporeal transmitter (voltage across the half-bridge) is set to drive the hysteresis of MLCCs #1, #2 and #3 over a specific voltage range for an inductive coupling factor k between 10 % and 30 % to optimize the stabilization of the secondary voltage U_{Load} over k. MLCC #1 is operated at a voltage between -22.4/+20.6 V and -25.8/+23.4 V, MLCC #2 between -16.9/+16.7 V and -19.1/+18.7 V, and MLCC #3 between -5.7/+5.5 V and -6.7/+6.4 V.

Using MLCCs #1, #2 and #3, a stabilization of the secondary voltage U_{Load} can be seen in Figure 3 for an inductive coupling factor k between about 10 % and 30 %. In the above-mentioned range of k, U_{Load} is between -11.4 % and +3.5 % around a median value of 20.2 V (17.9 - 20.9 V) using MLCC #1, between -15.6 % and +5.6 % around a median value of 16.0 V (13.5 - 16.9 V) using MLCC #2, and between -12.0 % and +4.0 % around a median value of 5.0 V (4.4 - 5.2V) using MLCC #3. In contrast, U_{Load} fluctuates between -77.4 % and +97.8 % around a median of 9.3 V (2.1V - 18.4 V) using the linear MLCC Linear 44 kHz above the system resonance frequency (see Figure 3, red).

A particularly high stabilization can be observed in Figure 3 of the secondary voltage U_{Load} between -1.2 % and +0.6 % around a median value of 17.3 V (17.1 - 17.4 V) for an inductive coupling factor $k \in [20\ \%, 30\ \%]$ using MLCC #1, ±0.9 % around a median value of 11.2 V (11.1 - 11.3 V) for $k \in [10\ \%, 18\ \%]$ using MLCC #2, and -1.6% and +2.6 % around a median value of 5.03 V (4.95 - 5.16 V) for $k \in [16\ \%, 30\ \%]$ using MLCC #3.

4 Conclusion

The experimental investigations in this paper have demonstrated the passive control of the IPT using the nonlinear properties of three ferroelectric MLCCs. The receiver circuit consists only of a parallel resonant circuit, a half-wave rectifier and a resistive load of 1200 Ω. The highest stabilization of the output voltage U_{Load} at the secondary load was achieved with the MLCC #2 with a variation of U_{Load} between ±0.9 % around a median value of 11.2 V at an inductive coupling factor k between 10 % and 18 %. Stabilization over the widest range of k between 16 % and 30 % was observed with the MLCC #3, however at the expense of poorer stabilization. Here, U_{Load} is between -1.6 % and +2.6 % around a median value of 5 V. In contrast to the linear MLCC Linear, the dependence of U_{Load} on k is significantly reduced using the ferroelectric nonlinear MLCCs #1, #2 and #3 (see Figure 3).

As a next step, we plan to use our physics-based model [13] to design a ferroelectric hysteresis to improve the stabilization of the secondary voltage U_{Load}. Ideally, U_{Load} should be kept constant over a given range of the inductive coupling factor k. In addition, stabilization should occur over the widest possible range of k, even for values of k less than 10 %, which is particularly relevant for IPT to neurostimulators.

Author Statement
Research funding: This work was supported by the Fraunhofer Center for Sensor Intelligence (ZSI). Conflict of interest: Authors state no conflict of interest.

References

[1] Jones CMP, Shaheed CA, Ferreira G, et al. Spinal Cord Stimulators: An Analysis of the Adverse Events Reported to the Australian Therapeutic Goods Administration. J Patient Saf 2022; 18: 507–511.

[2] Sette AL, Seigneuret E, Reymond F, et al. Battery longevity of neurostimulators in Parkinson disease: A historic cohort study. Brain Stimul 2019; 12: 851–857.

[3] Eastwood PR, Barnes M, MacKay SG, et al. Bilateral hypoglossal nerve stimulation for treatment of adult obstructive sleep apnoea. Eur Respir J 2020; 55.

[4] Nyxoah SA. Nyxoah Receives European CE Mark Approval for the Genio® System, a Disruptive Neurostimulation Solution for Obstructive Sleep Apnea Therapy. Mont-Saint-Guibert, Belgium 2019 Mar 20.

[5] Mashiach A, Scholz O, inventors. Method and device for treating sleep apnea.

[6] Coates S, Thwaites B. The Strength-Duration Curve and Its Importance in Pacing Efficiency: A Study of 325 Pacing Leads in 229 Patients. Pacing Clin Electrophysiol 2000; 23: 1273–1277.

[7] Cogan SF. Neural stimulation and recording electrodes. Annu Rev Biomed Eng 2008; 10: 275–309.

[8] Moisello E, Liotta A, Malcovati P, Bonizzoni E. Recent Trends and Challenges in Near-Field Wireless Power Transfer Systems. IEEE Open J. Solid-State Circuits Soc. 2023; 3: 197–213.

[9] Cheung T, Nuño M, Hoffman M, et al. Longitudinal impedance variability in patients with chronically implanted DBS devices. Brain Stimul 2013; 6: 746–751.

[10] Hong J, Pan F, Zhang Z, Teng J, He D. Constant current/voltage characteristics inductive power transfer system with variable static S-T/FC compensation. J. Power Electron. 2023.

[11] Wang Y, Mostafa A, Zheng Z, Zhang H, Zhu J, Lu F. Highly Misalignment-Tolerant Series-Series IPT System with Overcurrent and Overpower Protection for Underwater Manta Ray Robots. In: IEEE Wireless Power Technology Conference and Expo: IEEE; 2023. p. 1–6.

[12] Das CS, Shahee A, Lalla NP, Shripathi T. A simple and low cost Sawyer-Tower ferro-electric loop tracer with variable frequency and compensation circuit. Proceedings of the 54th DAE Solid State Physics Symposium 2009: 439.

[13] Olsommer Y, Ihmig FR, Rizzello G. Physics-based modeling of ferroelectric hysteresis for ceramic capacitors in inductively coupled microstimulators. IEEE Trans. Power Electron. 2024: 1–13.